

Article

Mesoporous Tungsten Oxides with Crystalline Framework for Highly Sensitive and Selective Detection of Foodborne Pathogens

Yongheng Zhu, Yong Zhao, Junhao Ma, Xiaowei Cheng, Jing Xie, Pengcheng Xu, Haiquan Liu, Hongping Liu, Haijiao Zhang, Minghong Wu, Ahmed A. Elzatahry, Abdulaziz Alghamdi, Yonghui Deng, and Dongyuan Zhao

J. Am. Chem. Soc., **Just Accepted Manuscript** • DOI: 10.1021/jacs.7b04221 • Publication Date (Web): 06 Jul 2017

Downloaded from <http://pubs.acs.org> on July 8, 2017

Just Accepted

“Just Accepted” manuscripts have been peer-reviewed and accepted for publication. They are posted online prior to technical editing, formatting for publication and author proofing. The American Chemical Society provides “Just Accepted” as a free service to the research community to expedite the dissemination of scientific material as soon as possible after acceptance. “Just Accepted” manuscripts appear in full in PDF format accompanied by an HTML abstract. “Just Accepted” manuscripts have been fully peer reviewed, but should not be considered the official version of record. They are accessible to all readers and citable by the Digital Object Identifier (DOI®). “Just Accepted” is an optional service offered to authors. Therefore, the “Just Accepted” Web site may not include all articles that will be published in the journal. After a manuscript is technically edited and formatted, it will be removed from the “Just Accepted” Web site and published as an ASAP article. Note that technical editing may introduce minor changes to the manuscript text and/or graphics which could affect content, and all legal disclaimers and ethical guidelines that apply to the journal pertain. ACS cannot be held responsible for errors or consequences arising from the use of information contained in these “Just Accepted” manuscripts.

Mesoporous Tungsten Oxides with Crystalline Framework for Highly Sensitive and Selective Detection of Foodborne Pathogens

Yongheng Zhu^{†, ‡, †}, Yong Zhao^{‡, †}, Junhao Ma[†], Xiaowei Cheng[†], Jing Xie[‡], Pengcheng Xu[†], Haiquan Liu[‡], Hongping Liu[‡], Haijiao Zhang[#], Minghong Wu[#], Ahmed A. Elzatahry[§], Abdulaziz Alghamdi[¶], Yonghui Deng^{*, †, †}, Dongyuan Zhao[†]

[†]Department of Chemistry, State Key Laboratory of Molecular Engineering of Polymers, Shanghai Key Laboratory of Molecular Catalysis and Innovative Materials, and iChEM, Fudan University, Shanghai 200433, China

[‡]College of Food Science and Technology, and Laboratory of Quality & Safety Risk Assessment for Aquatic Products on Storage and Preservation (Shanghai), Ministry of Agriculture, Shanghai Ocean University, Shanghai 201306, China

[†]State Key Laboratory of Transducer Technology, Shanghai Institute of Microsystem and Information Technology, Chinese Academy of Sciences, Shanghai 200050, China

[#]Institute of Nanochemistry and Nanobiology, School of Environmental and Chemical Engineering, Shanghai University, Shanghai 200444, China

[§]Materials Science and Technology Program, College of Arts and Sciences, Qatar University, PO Box 2713, Doha, Qatar

[¶]Department of Chemistry, College of Science, King Saud University, Riyadh 11451, Saudi Arabia

KEYWORDS mesoporous materials, tungsten oxide, templating synthesis, *listeria monocytogenes*, gas sensor

ABSTRACT: Foodborne pathogens like *Listeria monocytogenes*, can cause various illnesses and pose a serious threat to public health. They produce species-specific microbial volatile organic compounds, i.e. the biomarkers, making it possible to indirectly measure microbial contamination in foodstuff. Herein, highly ordered mesoporous tungsten oxides with high surface areas and tunable pores have been synthesized and used as sensing materials to achieve an exceptionally sensitive and selective detection of trace *Listeria monocytogenes*. The mesoporous WO₃-based chemiresistive sensors exhibit a rapid response, superior sensitivity, and highly selective detection of 3-hydroxy-2-butanone. The chemical mechanism study reveals that acetic acid is the main product generated by the surface catalytic reaction of the biomarker molecule over mesoporous WO₃. Furthermore, by using the mesoporous WO₃-based sensors, a rapid bacteria detection was achieved, with a high sensitivity, a linear relationship in a broad range, and a high specificity for *Listeria monocytogenes*. Such a good gas sensing performance foresees the great potential application of mesoporous WO₃-based sensors for fast and effective detection of microbial contamination for the safety of food, water safety and public health.

INTRODUCTION

Bacterial foodborne pathogens encompass various illnesses and continue to threaten public health all over the world.^[1] *Listeria monocytogenes* (LM) is one of the most hazardous bacteria. It can cause a fatal foodborne illness to pregnant women, neonates, and the elderly or immunocompromised people.^[2, 3] Additionally, LM can grow over a wide range of temperatures (0- 45 °C) and at high-salinity solutions. They have been widely found in environmental mediums (e.g. waters and sediments) and a variety of foods. Many countries have imposed a zero tolerance policy for LM since it has a low infectious dose (< 1000 cells) and high mortality rate.^[4] So far, various approaches for detection of pathogens have been proposed. Traditional methods including biochemical tests, cell culture, are standard modes but suffer the drawbacks of

intensive labor and time-consuming procedures.^[5, 6] In contrast, some newly developed detection techniques, such as the nucleic acid-based method and the immuno-based test can achieve significantly decreased detection time as compared with conventional techniques, they still require complex and expensive instruments highly trained personnel, and in some cases, they even give false positive results because they fail to distinguish dead or alive pathogens.^[7, 8] Therefore, it is of great interest and importance to develop an easy-to-perform, cheap, effective and convenient detection method for pathogenic bacteria in food, water and air which are closely related to people's safety and health.

It is well known that microorganisms including *Listeria monocytogenes* can produce species-specific microbial volatile organic compounds (MVOCs), which can be characterized as

1 biomarkers.^[9, 10] In recent years, the detection of MVOCs, i.e.
2 the indicators of microbial contamination, has emerged as a
3 novel and effective approach to reveal the microbial contami-
4 nation, owing to its ability to operate in a noninvasive and
5 rapid mode without the need for complex and expensive in-
6 struments and highly trained personnel.^[11 - 15] In this regard,
7 chemiresistive sensors based on semiconducting metal oxides
8 (SMOs) have attracted particular attention due to its ad-
9 vantages such as low-cost, convenient operation, fast response
10 and recovery process, and tunable responsivity to target gase-
11 ous molecules, making it possible to monitor the microbial
12 contamination indirectly by measuring the concentration of
13 relevant MVOCs.^[16]

14 However, the MVOCs produced by bacterial foodborne patho-
15 gens usually contain thousands of potentially interfering gas
16 species.^[17] It is challenging to adopt SMOs-based sensors to
17 sensitively and selectively detect trace target gases (sub-ppm
18 level) in exhaled gases of microorganisms like *Listeria mono-*
19 *cytogenes*.^[18] In order to achieve an enhanced gas sensing
20 performance, it is highly necessary to improve the surface-
21 chemisorbed oxygen species and gas transport kinetics in
22 SMOs-based sensors.^[19, 20] Ordered mesoporous SMOs with
23 high crystallinity, uniform and well-connected pores roughly
24 comparable to the mean free path of gas molecules can meet
25 both criteria.^[21 - 28] In this unique mesoporous architecture, the
26 high surface area can provide high density of active surface
27 sites, and numerous surface reactions can take place between
28 test gases and adsorbed oxygen species on the sensing layers,
29 improving the sensitivity of gas sensor.^[29, 30] Meanwhile, the
30 large porosity and good pore interconnectivity help to achieve
31 high sensitivity and selectivity by virtue of the good penetra-
32 tion of gas molecules dominated by Knudsen diffusion in the
33 mesoporous SMOs matrix.^[31, 32] To date, considerable efforts
34 have been directed toward synthesizing various ordered meso-
35 porous metal oxides through different approaches, such as
36 precipitation reactions,^[33] sol-gel process,^[34] spray pyrolysis,
37 ^[35] and chemical vapor deposition (CVD).^[36] These methods,
38 however, usually give rise to oxides with ill-defined structure,
39 poor crystallinity, and low porosity, which is unfavorable for
40 improved sensing performance.

41 In this study, highly ordered mesoporous tungsten oxides were
42 synthesized and used as semiconducting sensing materials to
43 sensitively and selectively detect of trace target biomarkers in
44 exhaled *Listeria monocytogenes* breath. The ordered mesopo-
45 rous WO₃ with different pore sizes were synthesized through a
46 ligand-assisted solvent evaporation induced co-assembly ap-
47 proach, by using diblock copolymer poly(ethylene oxide)-
48 block-polystyrene (PEO-*b*-PS) as a template, THF/ethanol
49 mixture as the solvent, and tungsten chloride as tungsten pre-
50 cursors in the presence of acetylacetonate (AcAc). Notably,
51 acetylacetonate was employed as a coordination agent to retard
52 the hydrolysis and condensation of tungsten precursor by sta-
53 bilizing the hydrolyzed tungsten hydroxide sol, which makes
54 the assembly process controllable. After co-assembly, pyroly-
55 sis treatment of the mesostructural composites in inert atmos-
56 phere and finally calcination in air, ordered mesoporous tung-
57 sten oxides with a face-centered cubic (fcc) structure were
58 obtained. By changing the hydrophobic PS segment length of
59 the template, the crystalline mesoporous WO₃ can be readily
60 tailored with tunable pore size of 10.6 - 15.3 nm, high surface
area of 76 - 136 m²/g, and adjustable pore volume of 0.13 -

0.17 cm³/g, respectively. The mesoporous WO₃-based sensor
for foodborne pathogens show a rapid response (< 10 s), supe-
rior sensitivity ($R_{\text{air}} / R_{\text{gas}} > 50$), and highly selective detection
against specific target gases at the sub-ppm level, due to their
good merits of suitable pore size, high surface area and active
site-rich pore walls. Furthermore, by using the mesoporous
WO₃-based sensor, a rapid bacteria detection was achieved in
1 min with a high sensitivity of 10 CFU mL⁻¹, a good linear
relationship in the range of 10 - 10⁶ CFU mL⁻¹, and a high
specificity for *Listeria monocytogenes* in the presence of 10⁶
CFU mL⁻¹ *Vibrio parahaemolyticus* or *Escherichia coli*. It
opens up the possibility for the mesoporous WO₃-based sensor
to be used as a new platform to conveniently and effectively
detect *Listeria monocytogenes* in food, water and so on.

EXPERIMENTAL SECTION

Chemicals and Materials. Chemicals and solvents of analyti-
cal grade were purchased and used as received. Monomethox-
ypoly (ethylene oxide) (Mw: 5000 g / mol) (designed as PEO-
5000) was purchased from Aldrich. 2-bromoisobutyl bromide
and Copper (I) bromide were purchased from Alfa Aesar.
N, N, N', N', N''-Pentamethyl-diethylenetriamine (PMDETA)
was purchased from Acros. Pyridine (AR) and Al₂O₃ (FCP)
were purchased from Shanghai Chemical Reagent Co. Ltd.
Tetrahydrofuran (THF), ethanol, styrene, anhydrous ethylether,
petroleum ether (30 - 60 °C), WCl₆, acetylacetonate (AcAc) and
WO₃ nanoparticles of AR grade were purchased from Sino-
Pharm Chemical Reagent Co. Ltd. All gases were purchased
from Dalian Date Gas Co. Ltd, and their purity was up to
99.5%.

Synthesis of Ordered Mesoporous WO₃. The amphiphilic
PEO-*b*-PS diblock copolymers with different molecular
weight were prepared by atom transfer radical polymerization
(ATRP) method reported previously.^[37] In a typical synthesis
of ordered mesoporous WO₃, PEO₁₁₇-*b*-PS₁₈₆ (100 mg) was
firstly dissolved in THF (5.0 g) to form a clear solution in a
glass vial, forming the solution A. 0.25 g of WCl₆ was dis-
solved in 0.5 g of ethanol and 0.25 g of acetylacetonate (AcAc),
forming the solution B. The above two solutions were then
mixed with stirring at room temperature for 2 h, giving rise to
a yellow-green homogeneous solution. The obtained solution
was cast onto petri dishes, followed by evaporation of the sol-
vent at room temperature for 1 - 2 h and annealing at 100 °C
for 24 h, and the inorganic - polymer composite was obtained.
After that, the hybrids film was collected and ground into
powders, followed by pyrolysis at 350 °C in N₂ for 3 h and
then at 500 °C for 2 h (the ramp rate is 1 °C min⁻¹). Finally,
the as-made carbon-supported mesoporous tungsten oxide
samples were further calcined at 500 °C in air for 2 h, and
yellow-green mesoporous tungsten oxides were obtained.
Through the same synthesis procedure, PEO₁₁₇-*b*-PS₂₃₂, and
PEO₁₁₇-*b*-PS₂₉₇ copolymers were also used as templates to
synthesize mesoporous WO₃.

Gas sensing properties of the gas sensor.

The obtained mesoporous WO₃ materials were grounded with
terpineol to form a paste which was coated onto the surface of
ceramic tubes printed with Au electrodes and Pt wires in ad-
vance. After sintering at 500 °C for 2 h, a Ni-Cr alloy coil was
inserted into the tube as a heater to control the operating tem-
perature of the sensors. To enhance the stability, the as-
fabricated sensors were annealed at 290 °C for one week.

1 A static test system was employed to measure the gas response
2 of the sensor. As shown in Figure S1, in measuring the electric
3 circuit for gas sensor, a load resistor (R_L) was connected in the
4 series with it. Herein, R_L and the circuit voltage (V_C) was a
5 constant, and the voltage of the load resistor (V_{out}) was record-
6 ed once in every second. In a typical sensing process, the test
7 gas such as 3-hydroxy-2-butanone was injected into a chamber
8 and diluted with air. The test gas can react with the adsorbed
9 oxygen species in mesoporous WO_3 sensing layers and release
10 free electrons, decreasing the resistance and the voltage of the
11 sensor, while the V_{out} was increased. The response of the sensor
12 was defined as R_a/R_g , where R_a and R_g stand for the resis-
13 tance of the sensor in air and in the test gas, respectively.
14 The response time or recovery time is counted as the time
15 taken by the sensor output to achieve 90% of the total resis-
16 tance change after injecting or releasing the test gas.

16 Gas chromatograph-mass spectrometer (GC-MS, Agilent
17 7890A-5975C) was used to analyze the gases produced in the
18 sensing experiment. The GC-MS is equipped with a DB-17
19 MS capillary column (30 m \times 0.25 mm \times 0.25 mm). The ex-
20 periment was carried out as follows. The GC oven temperature
21 was first held at 40 $^{\circ}C$ for 4 min, then gradually increased to
22 280 $^{\circ}C$ with a ramping rate of 15 $^{\circ}C$ min^{-1} to and finally held
23 for 16 min. The 0.5 mL sample solution was injected into GC
24 at the split ratio of 50 : 1, and the flow-rate of the He carrier
25 gas is 33 mL min^{-1} . The quad-rupole temperature is 150 $^{\circ}C$
26 and the source temperature is 230 $^{\circ}C$. Ionization voltage is 70
27 eV. The mass spectrometer was acquired in the m/z range of
28 20 - 500. MS analysis is performed in electron impact (EI)
29 mode. The product composition identification was based on
30 the comparison of MS data using a mass spectral library
(NIST08).

31 **Bacteria cultures**

32 The *Listeria monocytogenes* (ATCC 7644) cultures were pur-
33 chase from the American Type Culture Collection (ATCC).
34 And then the bacteria were spread onto the PALCAM Medium
35 plate for 24 h at 37 $^{\circ}C$ for activation. Before use, *Listeria*
36 *monocytogenes* inoculum was incubated in 10 ml of tryptic
37 soy broth and grown overnight (18 to 24 h) at 37 $^{\circ}C$ in a gyra-
38 tory shaker at 180 r/min. Then the culture was diluted to 10^1 ,
39 10^2 , 10^3 , 10^4 , 10^5 , 10^6 CFU mL^{-1} . The sensor S_d based on mes-
40 oporous WO_3 -PEO₁₁₇-*b*-PS₁₈₆ was used to detect the diluted
41 samples with different concentration, after which were incuba-
42 tion for 2 – 18 h every two hours at 30 $^{\circ}C$.

42 **The variability in extent of *Listeria monocytogenes* growth.**

43 The growth variability of *Listeria monocytogenes* was ob-
44 tained using a method based on turbidity measurements. In a
45 typical process, 200 μL bacterial suspensions of an initial con-
46 centration of approximately 10^1 , 10^2 , 10^3 CFU mL^{-1} were in-
47 oculated TSB at 37 $^{\circ}C$, which were transferred into 100-well
48 microtiter plates. The turbidity corresponding optical density
49 (OD) values was obtained with the automated turbidimetric
50 system Bioscreen C (Oy Growth Curves Ab Ltd., Raisio, Fin-
51 land), and the absorbance at 580 nm using the wide band filter.
52 In order to obtain the turbidity growth curves, the OD values
53 were record every 30 min for up to 18 h. Every experiment is
54 repeated three times in this process.

54 **Standard plate count method.**

55 To obtain the amount of the alive and active *Listeria mono-*
56 *cytogenes*, the plate counting method was used. The total aer-
57 obic bacteria were obtained after serially diluted samples (10^1 ,

10^2 , 10^3 CFU mL^{-1}) were plated on TSA (TSB with 18 g/L
agar added). Colonies were counted after the plates incubated
at 37 $^{\circ}C$ for 48 ± 2 h. Growth curves were obtained by plotting
log CFU mL^{-1} against the exposure time. Three trials with
three replicates per trial were done.

55 **Measurement and Characterization.**

56 Prior to measurements, all the block copolymer samples were
57 dissolved in the $CDCl_3$. 1H NMR spectra was performed over
58 a DMX 500 MHz spectrometer (Bruker, Germany) with tet-
59 ramethylsilane as the internal standard (Figure. S2A, B). Gel-
60 permeation chromatography was operated on an Agilent 1100
GPC system with a refractive index detector (Figure. S2C).
The small-angle X-ray scattering (SAXS) patterns were col-
lected on a Nanostar U SAXS system (Bruker, Germany),
using Cu $K\alpha$ radiation (40 kV, 35 mA). The structural charac-
teristics of the mesoporous WO_3 were determined by powder
X-ray diffraction (XRD) analysis, using a Bruker D4 X-ray
diffractometer (Germany) with Ni-filtered Cu $K\alpha$ radiation (40
kV, 40 mA, 1.54056 \AA). High-resolution scanning electron
microscopy (HR-SEM, Hitachi S4800) was operated at 1 kV
and 10 μA . Transmission electron microscopy (TEM, JEM-
2100 F) was operated at accelerating voltage of 200 kV. The
nitrogen adsorption was measured at 77 K using a Micromeritics
Tristar 3020 analyzer (USA). The specific surface areas
were calculated with the Brunauer-Emmett-Teller (BET)
method, using the adsorption data at $P/P_0 = 0.02 - 0.20$. The
pore volumes and pore size distributions were derived from
the adsorption branches of isotherms, and the window-size
was calculated from desorption branch, using the Broekoff-de
Boer (BdB) sphere model. A Dilor Lab Ram-1B microscopic
Raman spectrometer (France) was utilized to obtain Raman
spectra of the samples, equipped with a He-Ne laser working
at wavelength of 632.8 nm. X-ray photoelectron spectroscopy
(XPS, PHI-5000C ESCA) was used to determine the surface
composition of the products, operating with Mg $K\alpha$ radiation
($h\nu = 1253.6$ eV) or Al $K\alpha$ radiation ($h\nu = 1486.6$ eV). Bind-
ing energy values were charge corrected to the adventitious
carbon (C 1s = 284.6 eV).

59 **RESULTS AND DISCUSSION**

60 The lab-made amphiphilic PEO-*b*-PS copolymers with the
same PEO segment length but different PS chain lengths
(PEO₁₁₇-*b*-PS₁₈₆, PEO₁₁₇-*b*-PS₂₃₂ and PEO₁₁₇-*b*-PS₂₉₇), were
prepared via atom transfer radical polymerization (ATRP)
approach.^[38] By virtue of the supporting effect of carbon resi-
dues from the macromolecular template PEO-*b*-PS during
carbonization in an inert atmosphere, the resulting carbon spe-
cies can prevent the collapse of mesostructured walls during
high-temperature crystallization of titania and niobia.^[39 - 41]
Crystalline ordered mesoporous WO_3 materials with different
pore size were synthesized through a ligand assisted solvent
evaporation induced co-assembly approach by using home-
made amphiphilic PEO-*b*-PS as the template molecules, tung-
sten chloride as a precursor in the presence of acetylacetone
(Figure. 1). The water-insoluble PEO-*b*-PS copolymer was
well dissolved in THF solution, and then the solution was
mixed with an ethanolic solution containing WCl_6 and acety-
lacetone (AcAc), forming the $WCl_{6-x}(AcAc)_x$ compounds due
to the strong complexation of AcAc with tungsten ions by
coordination bonds and thus can significantly retard their hy-
drolysis. It favors the co-assembly of the diblock copolymer

and the inorganic precursors, avoiding phase separation between them in a much wide range of synthesis conditions even in the humidity of 15-85%. As THF evaporates from the precursor solution, amphiphilic PEO-*b*-PS copolymers co-assemble with tungsten species into ordered mesostructured composites which were further subjected to pyrolysis treatment in N₂ at 350 °C and calcination at 500 °C in air to remove the template, resulting in ordered mesoporous WO₃ materials. By using PEO-*b*-PS copolymers with different molecular weights, a series of mesoporous WO₃ samples can be obtained and denoted as WO₃-PEO_x-*b*-PS_y, wherein x and y represent the numbers of repeating unit of ethylene oxide and styrene, respectively.



Figure 1. Schematic illustration of the formation of ordered mesoporous WO₃ materials via the solvent evaporation induced co-assembly approach. **Step 1.** With the evaporation of THF, the PEO_x-*b*-PS_y copolymers can co-assemble with tungsten species to form spherical composite micelles with hydrophobic PS core surrounded by a shell of hybrid PEO-AcAc-stabilized tungsten species. **Step 2.** With the continuous evaporation of THF, the composite spherical micelles further co-assemble into 3-D ordered mesostructure which was fixed by annealing at 100 °C for 24 h. **Step 3.** The as-made inorganic-polymer hybrid was calcined in N₂ at 350 °C, leading to carbon-supported mesoporous WO₃ materials. **Step 4.** Ordered mesoporous WO₃ materials are finally obtained after removal of the supporting carbon in the pore channel via calcination in air at 500 °C.

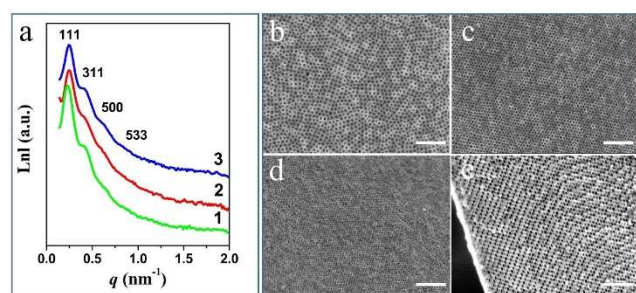


Figure 2. (a) SAXS patterns of the WO₃-PEO_x-*b*-PS_y samples of WO₃-PEO_x-*b*-PS_y samples obtained after carbonization in N₂ at 350 °C and calcination at 500 °C in air (1, WO₃-PEO₁₁₇-*b*-PS₂₉₇, 2, WO₃-PEO₁₁₇-*b*-PS₂₃₂, 3, WO₃-PEO₁₁₇-*b*-PS₁₈₆). FESEM images of WO₃-PEO_x-*b*-PS_y samples: (b, surface) WO₃-PEO₁₁₇-*b*-PS₂₉₇, (c, surface; e, cross-section) WO₃-PEO₁₁₇-*b*-PS₂₃₂, and (d, surface) WO₃-PEO₁₁₇-*b*-PS₁₈₆. Scale bars, 500 nm.

Small-angle X-ray scattering (SAXS) patterns of the mesoporous WO₃-PEO₁₁₇-*b*-PS₁₈₆ after calcination at 500 °C in air to remove the templates, are similar to those of WO₃-PEO₁₁₇-*b*-PS₂₃₂ and WO₃-PEO₁₁₇-*b*-PS₂₉₇ (Figure. 2a). The well-resolved four scattering peaks with *q*-values of 0.249, 0.434, 0.718, and 0.943 nm⁻¹, respectively, can be exactly indexed as the 111, 311, 500 and 533 reflections, corresponding to ordered face-centered cubic (*fcc*) mesostructure (space group *Fm3m*).^[42] Due to the longer PS chain length of PEO₁₁₇-*b*-PS₂₉₇, the scattering peaks of the sample WO₃-PEO₁₁₇-*b*-PS₂₉₇ shift to lower *q* values compared to the sample WO₃-PEO₁₁₇-*b*-PS₁₈₆. The former has a unit cell parameter of 47.3 nm, larger than that of the latter (43.5 nm), implying a larger building block formed by PEO₁₁₇-*b*-PS₂₉₇.

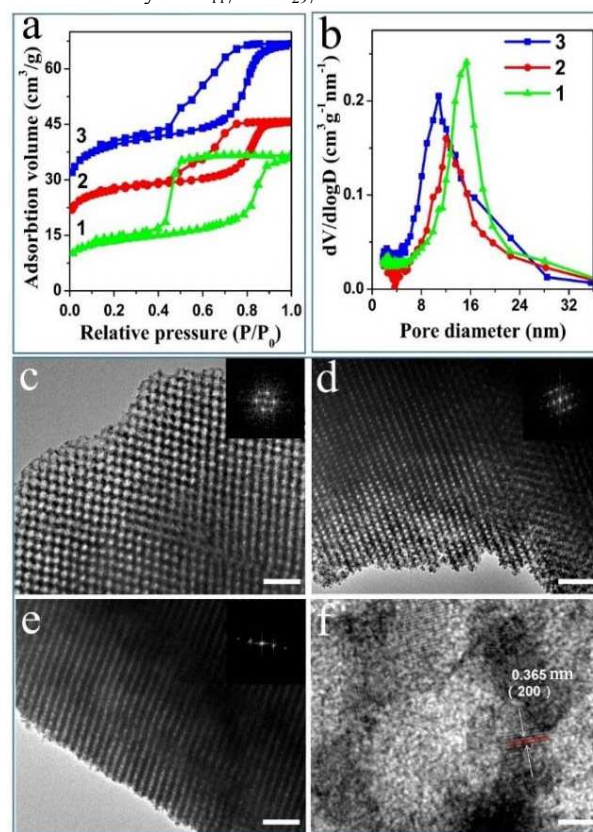


Figure 3. (a) Nitrogen adsorption-desorption isotherms and (b) the corresponding pore size distributions of WO₃-PEO_x-*b*-PS_y samples obtained after carbonization in N₂ at 350 °C and calcination at 500 °C in air (1, WO₃-PEO₁₁₇-*b*-PS₂₉₇, 2, WO₃-PEO₁₁₇-*b*-PS₂₃₂, 3, WO₃-PEO₁₁₇-*b*-PS₁₈₆). TEM images of taken along (c) [100] and (d) [211] (e) [110] directions. (f) HRTEM image of WO₃-PEO₁₁₇-*b*-PS₂₃₂ after carbonization in N₂ at 350 °C and calcination at 500 °C in air. The insets in (c), (d), and (e) are the corresponding fast FFT images. Scale bars, 100 nm (c, d and e), 5 nm (f).

The HR-SEM images taken along both the surface and cross section of the samples clearly show that all mesoporous WO₃ materials possess a highly ordered mesostructure with a uniform pores (Figure. 2b - e). It implies a spherical packing process of the composite micelles of PEO-*b*-PS/tungsten species during the co-assembly process. TEM images (Figure. 3c-e) show that the obtained mesoporous WO₃ sample (WO₃-PEO₁₁₇-*b*-PS₂₃₂) has a high degree of periodicity viewed from

[100], [211], and [110] directions, respectively. It further confirms the WO₃ mesostructure templated from the copolymer PEO₁₁₇-*b*-PS₂₃₂ has a highly ordered cubic symmetry (*Fm3m*). The uniform and tunable pores with a size of about 12.3 nm can clearly be observed in the TEM images of the sample WO₃-PEO₁₁₇-*b*-PS₁₉₈ (Figure. 3c), agreeing well with the N₂ sorption results. The unit cell parameter is estimated from TEM images to be about 35.2 nm, which is in good agreement with that (35.6 nm) from SAXS data. HR-TEM images (Figure. 3f) clearly shows the crystal lattice, implying that the pore wall consists of well crystallized and interconnected WO₃ nanoparticles corresponding to the different crystal plane. The lattice spacing is about 0.365 nm, corresponding to the (200) planes of monoclinic WO₃.^[44] As measured from Figure 3f, the crystal size of the crystallized and interconnected WO₃ nanoparticles corresponding to the (200) planes is about 11.0 nm. While the crystal size of well crystallized and interconnected WO₃ nanoparticles corresponding to the (200) planes is about 11.5 nm calculated from the XRD patterns (Figure. S4) by Scherrer equation, matching well with the HR-TEM data.

The structure and bonding of WO₃-PEO_{*x*}-*b*-PS_{*y*} samples were characterized by XRD spectroscopy. The XRD pattern displays well-resolved diffraction peaks in the range of 10 - 60 degree (Figure. S4), matching well with the crystalline monoclinic phase of WO₃ with lattice parameters of *a* = 0.7297, *b* = 0.7539, *c* = 0.7688 nm and β = 90.918 (JCPDS No. 43-1035). No diffraction peaks from other crystalline impurities were observed, suggesting a pure crystalline phase. The broadening of the diffraction peaks can be ascribed to the WO₃ nanocrystals in the pore wall.^[45] To determine the exact composition and the oxidation state of the W species, X-ray photoelectron

spectroscopy (XPS) analysis was performed on the obtained mesoporous WO₃ (Figure. S5). All peaks can be indexed to W and O elements, indicating the high purity of as-synthesized sample. The high-resolution XPS spectra of W 4f is present in Figure. S5a. The peaks at binding energies of 35.6 and 37.7 eV match well with the reported values for the W⁶⁺ oxidation state.^[4] The O 1s peak could be resolved to the two Gaussian function peaks at 530.7 and 531.3 eV for the mesoporous WO₃ (Figure. S5b). The state of O 1s indicates two types of oxygen in the surface, i.e. the lattice oxygen (O²⁻) and the adsorbed oxygen (O⁻ and O₂⁻). Usually, the lattice oxygen hardly interacts with the reducing gas and thus cannot contribute to the generation of the main charge-carriers in n-type semiconductors; while the adsorbed oxygen is very active and can react with reducing gases, changing the concentration of main carriers.^[46] All the WO₃-PEO_{*x*}-*b*-PS_{*y*} samples exhibit typical Raman adsorption bands of 273, 327, 715 and 807 cm⁻¹, which are similar to those of the commercial tungsten oxide powder and can be identified as the four strong modes of tungsten oxides (Figure. S6).^[47] The Raman bands at 273 and 327 cm⁻¹ correspond to the O-W-O bending modes of bridging oxygen, and the bands at 715 and 807 cm⁻¹ can be attributed to stretching modes. It is worth noting that, compared with the commercial bulk WO₃, the Raman adsorption peaks became broader gradually from WO₃-PEO₁₁₇-*b*-PS₂₉₇ to WO₃-PEO₁₁₇-*b*-PS₂₃₂ and to WO₃-PEO₁₁₇-*b*-PS₁₈₆ with increasing specific surface areas (Figure. S6b-d). It implies a continuous increase of the density of crystal defects and oxygen vacancies, which is directly relevant to the catalytic activity and gas sensing property of semiconductors.^[48]

Table 1. The texture properties and sensing performance of the obtained WO₃-PEO_{*x*}-*b*-PS_{*y*} and commercial WO₃ particles

Samples	BET surface area (m ² /g)	Total pore volume (cm ³ /g)	Pore size (nm) ^a	Sensitivity (R _d /R _g) ^b	Response/Recovery ^c (s)
commercial WO ₃	6	/	/	6.2	18.0 / 43.0
WO ₃ -PEO ₁₁₇ - <i>b</i> -PS ₂₉₇	76	0.17	15.3	32.7	12.0 / 30.0
WO ₃ -PEO ₁₁₇ - <i>b</i> -PS ₂₃₂	95	0.15	12.1	46.2	10.0 / 26.0
WO ₃ -PEO ₁₁₇ - <i>b</i> -PS ₁₈₆	136	0.13	10.6	56.1	4.0 / 13.0

^aThe pore sizes were derived from the adsorption branches of the isotherms by using the BJH method. ^bThe sensitivity of sensors S_a, S_b, S_c, and S_d to 3-hydroxy-2-butanone at 25 ppm, and the S_a, S_b, S_c, and S_d are based on commercial WO₃ particles, WO₃-PEO₁₁₇-*b*-PS₂₉₇, WO₃-PEO₁₁₇-*b*-PS₂₃₂, and WO₃-PEO₁₁₇-*b*-PS₁₈₆, respectively. ^cThe response and recovery of S_a, S_b, S_c, and S_d to 3-hydroxy-2-butanone at 5 ppm.

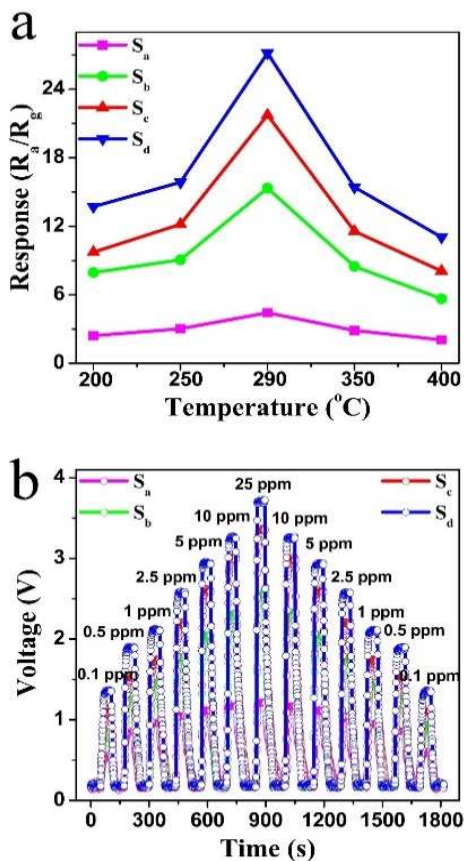


Figure 4. Typical response curve and variations of the sensors base on different samples (S_a , S_b , S_c , and S_d based on commercial WO_3 particles, WO_3 -PEO₁₁₇-*b*-PS₂₉₇, WO_3 -PEO₁₁₇-*b*-PS₂₃₂, and WO_3 -PEO₁₁₇-*b*-PS₁₈₆, respectively). (a) The responses vs the operating temperature to 5 ppm of 3-hydroxy-2-butanone, (b) the responses vs 3-hydroxy-2-butanone at with concentrations of 0.1 - 25 ppm measured at 290 °C

As one of the most interesting and important metal oxides, WO_3 has attracted much attention because of its excellent gas sensitivity.^[49, 50] Mesoporous WO_3 materials with a high porosity have unique advantages of short gas diffusion length, high carrier mobility, and high specific surface area that facilitates the adsorption and desorption of analyte molecules. Previous study has revealed that the main MVOCs produced by *Listeria monocytogenes* is 3-hydroxy-2-butanone (32.2% in abundance of the MOVs), and its concentration in MVOCs increased with the growth of *Listeria monocytogenes*.^[51] Therefore, 3-hydroxy-2-butanone can be considered as a marker volatile chemical for predicting the cell number of *Listeria monocytogenes*. In this study, we systematically investigated the application possibility of our mesoporous WO_3 -PEO_{*x*}-*b*-PS_{*y*} materials for indirectly sensing detection of *Listeria monocytogenes* by measuring the concentration of 3-hydroxy-2-butanone in their MVOCs. We first fabricated four series of gas sensors, S_a , S_b , S_c , and S_d , based on commercial WO_3 , WO_3 -PEO₁₁₇-*b*-PS₂₉₇, WO_3 -PEO₁₁₇-*b*-PS₂₃₂, and WO_3 -PEO₁₁₇-*b*-PS₁₈₆, respectively, to examine their responses toward 3-hydroxy-2-butanone.

Since the gas sensing properties of semiconductors usually depend on the working temperature,^[52, 53] the sensors based on

commercial bulk WO_3 particles and mesoporous WO_3 -PEO_{*x*}-*b*-PS_{*y*} samples were first tested in 5 ppm of 3-hydroxy-2-butanone at different operating temperatures of 200 - 400 °C (Figure. 4a). The response of all sensors exhibited a high response to target gas at 290 °C. It implies that the equilibrium density of chemisorbed oxygen ions on WO_3 is maximized at this temperature. Thus, 290 °C was adopted as the working temperature for subsequent detections. All the fabricated gas sensors show continuous increasing responses to 3-hydroxy-2-butanone in a wide concentration ranging from 0.1 to 25 ppm (Figure. 4b). Even at a low concentration of 0.1 ppm, the sensitivity can reach 5.3, 8.7 and 13.5 for the Sensor S_b , S_c , S_d , respectively, and the response values increase with the gas concentration. Moreover, these sensors show excellent reversibility and repeatability as the concentration decreased from 25 to 0.1 ppm. Notably, the sensitivity was found to increase dramatically with the specific surface areas of tungsten oxides (Table 1), and the maximal response was 56.1 at 25 ppm of 3-hydroxy-2-butanone for S_d based on the mesoporous WO_3 -PEO₁₁₇-*b*-PS₁₈₆. The highest response is mainly due to its largest surface area (135 m²/g), which provides the highest density of active surface sites for numerous surface reactions between test gases and adsorbed oxygen species on the sensing layers can take place. Moreover, the response of S_d is nearly 9 times higher than that of S_a based on the commercial WO_3 . It suggests that the sensitivity can be significantly increased by fabricating ordered mesoporous structure.

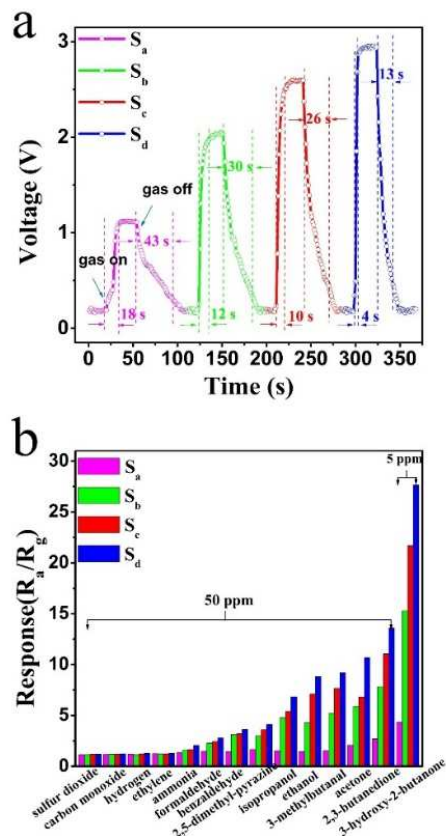


Figure 5. (a) Response and recovery curve of the sensors base on different samples (S_a , S_b , S_c , and S_d based on commercial WO_3 particles, WO_3 -PEO₁₁₇-*b*-PS₂₉₇, WO_3 -PEO₁₁₇-*b*-PS₂₃₂, and WO_3 -PEO₁₁₇-*b*-PS₁₈₆, respectively) to 5 ppm 3-hydroxy-2-butanone. (b) Responses of

the above four sensors to interfering gases at 50 ppm, 3-hydroxy-2-butanone at 5 ppm, respectively.

The response and recovery behaviors are an important parameter for evaluating the performance of the sensing materials. The continuous dynamic electrical response of the sensors to 5 ppm of 3-hydroxy-2-butanone is shown in Figure. 5a. The sensor S_d based on the sample WO_3 -PEO₁₁₇-*b*-PS₁₈₆ exhibits a markedly higher response upon exposure to 3-hydroxy-2-butanone (response = 4.0 s, recovery = 13.0 s) compared to those of commercial WO_3 nanoparticles (response = 18.0 s, recovery = 43.0 s), WO_3 -PEO₁₁₇-*b*-PS₂₉₇ (response = 12.0 s, recovery = 30.0 s), and WO_3 -PEO₁₁₇-*b*-PS₂₃₂ (response = 10.0 s, recovery = 26.0 s). As the resistive sensor is based on surface effects, the higher specific surface area of the mesoporous WO_3 -PEO₁₁₇-*b*-PS₁₈₆ can provide more adsorption sites for sensing reactions in the solid-gas interfaces, resulting in the highest response (4.0 s) of sensor S_d upon exposure to the same concentration target gas. On the other hand, since the WO_3 -PEO₁₁₇-*b*-PS₁₈₆ sample has larger pore window size (6.3 nm) than that of the mesoporous WO_3 -PEO₁₁₇-*b*-PS₂₃₂ (5.4 nm) and WO_3 -PEO₁₁₇-*b*-PS₂₉₇ (3.5 nm), gas molecules can more rapidly and readily diffuse within the whole porous structure in S_d , resulting in the highest recovery (13.0 s) of sensor S_d in the target gas of the same concentration.

The analysis of species-specific microbial volatile organic compounds (MVOCs) produced by microorganisms requires not only high sensitivity, fast response and recovery, but also high selectivity. In order to investigate the selectivity of the mesoporous WO_3 -based sensors, we also measured their response to different gases at 50 ppm, such as carbon monoxide, ethylene, ethanol and acetone at 290 °C. As shown in Figure. 5b, sensor S_d based on the sample WO_3 -PEO₁₁₇-*b*-PS₁₈₆ exhibited excellent selectivity to 3-hydroxy-2-butanone at 5 ppm and little interference from other gases. More importantly, four typical gases in exhaled *Listeria monocytogenes* breath, 2, 3-butanedione (11.6 % in abundance of the MOVs), 3-methylbutanal (10.1 % in abundance of the MOVs), 2, 5-dimethyl-pyrazine (10.4 % in abundance of the MOVs) and benzaldehyde (17.6 % in abundance of the MOVs) were also selected as interfering gases.^[51] As shown in Figure. 5b, the response value of the sensor S_d to 3-hydroxy-2-butanone at 5 ppm is at least 3 times higher than that for the four selected interfering gases even at 50 ppm. More strikingly, the response value of S_d to 5 ppm of 3-hydroxy-2-butanone (32.2% in abundance of the MOVs) is more than 10 times higher than that for benzaldehyde (17.6 % in abundance of the MOVs) at 50 ppm. These results clearly indicate that our sensors have superior selectivity to 3-hydroxy-2-butanone in exhaled *Listeria monocytogenes* breath. The stability study on our mesoporous WO_3 -based gas sensors revealed that the sensors' response to 5 ppm of 3-hydroxy-2-butanone show a negligible change of less than 3% after working continuously for 35 days (Figure. S7), reflecting a good long-term stability of mesoporous WO_3 sensors. All the results clearly show that the sensor S_d based mesoporous WO_3 -PEO₁₁₇-*b*-PS₁₈₆ exhibits excellent comprehensive performance with high selectivity and sensitivity to 3-hydroxy-2-butanone. It has a good stability, quick response and recovery dynamics, which is important for practical applications.

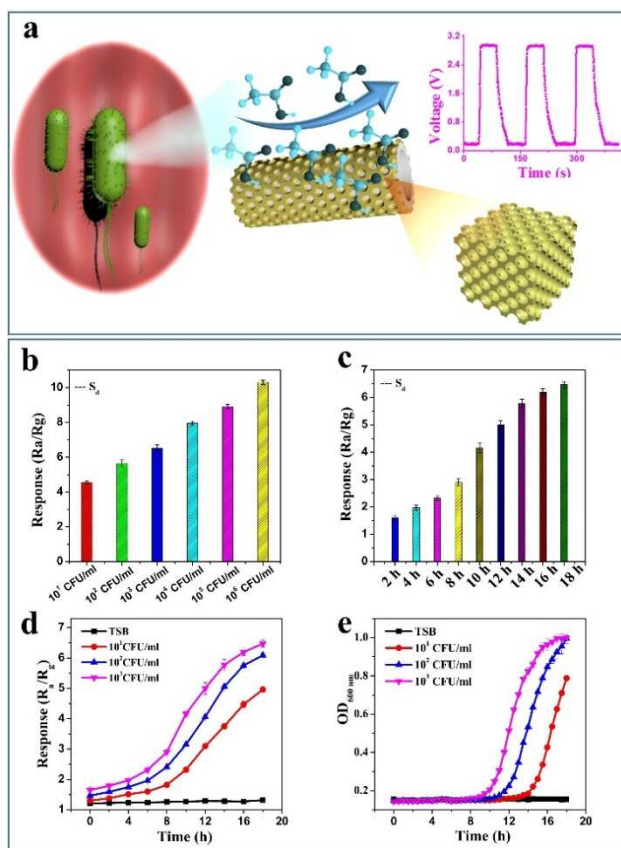


Figure 6. (a) Schematic diagram of the principle for detection of *Listeria monocytogenes* using the sensor S_d based WO_3 -PEO₁₁₇-*b*-PS₁₈₆. (b) Typical response of the S_d to various concentrations of *Listeria monocytogenes* after incubated at 30 °C for 18 h. (c) Typical response of the S_d to 10^3 CFU mL⁻¹ *Listeria monocytogenes* which were incubated for 2 - 18 h at 30 °C. (d) The sensitivity of the S_d to various concentrations of *Listeria monocytogenes* (10^1 , 10^2 , 10^3 CFU mL⁻¹, respectively) measured at an interval of 2 h during 18 h incubation at 30 °C and the control sample of tryptone soy broth medium (TSB). (e) The variability of *Listeria monocytogenes* growth was obtained every 30 min for up to 18 h in wells inoculated with 200 μ L bacterial suspensions of an initial concentration of 0, 10^1 , 10^2 , 10^3 , CFU mL⁻¹, using a method based on turbidity measurements.

The above exciting results drive us to further explore the possibility to employ the ordered mesoporous WO_3 based gas sensors for indirect monitoring and detection of bacteria. Figure. 6a schematically illustrates the principle for detection of *Listeria monocytogenes* using sensor S_d based on WO_3 -PEO₁₁₇-*b*-PS₁₈₆. Sensor S_d was firstly exposed to various concentrations of *Listeria monocytogenes* (initial concentrations: 10^1 to 10^6 CFU mL⁻¹, incubation for 18 h). The results (Figure. 6b) clearly reveal that the response of sensor S_d is directly proportional to the concentration of bacteria, showing a much higher sensitivity ($R_{air} / R_{gas} = 10.3$) upon exposure to 10^6 CFU mL⁻¹ bacteria than that ($R_{air} / R_{gas} = 4.9$) for the case of 10^1 CFU mL⁻¹ bacteria. Subsequently, similar study was carried out by exposing sensor S_d in *Listeria monocytogenes* solution (10^3 CFU mL⁻¹) during incubation for 2 - 18 h, and the response was also measured. After incubation for 2 h, the sensor shows large voltage signal change, which is due to the increas-

ing accumulation of MVOCs concentration caused by the continuous growth of microbial cells (Figure. 6c).

Furthermore, the variability in extent of microbial growth was measured by using both chemiresistive sensing method based on sensor S_d (Figure. 6d) and the conventional turbidity method (Figure. 6e). It can be seen that the variability of *Listeria monocytogenes* is detected using S_d even for a low concentration of 10^1 CFU mL⁻¹ after incubation for only 2 h, and the amount of the alive and active bacteria is 1.61 Log₁₀ CFU/mL (Figure. S8). By contrast, the turbidity method failed to detect the variability even for a high concentration of 10^3 CFU mL⁻¹ *Listeria monocytogenes* after incubation for 8 h, corresponding to an amount of the alive and active bacteria of 4.93 Log₁₀ CFU/mL (Figure. S8). These results indicate that our sensor S_d is more sensitive and can detect the bacteria more quickly and conveniently. More importantly, the data obtained using our sensor reflect the variability of microbial growth of alive and active bacteria which are the only source of the biomarker molecule (i.e. 3-hydroxy-2-butanone) and should be monitored and evaluated for the safety of food, water safety and public health in practical applications. The selectivity of sensors to bacteria is also very important in detection of foodborne pathogens. Two other kinds of typical bacteria, *Vibrio parahaemolyticus* and *Escherichia coli* were also evaluated. As shown in Figure. S9, the response of S_d upon exposure to 10^6 CFU mL⁻¹ *Vibrio parahaemolyticus* or *Escherichia coli* is much lower than the response for the case of 10^3 CFU mL⁻¹ *Listeria monocytogenes*, suggesting a highly selective recognition for *Listeria monocytogenes*. All these results clearly indicate that the mesoporous WO₃-based sensors possess excellent sensing performance in detecting active *Listeria monocytogenes* with high sensitivity and precision, good convenience and selectivity.

The gas-sensing mechanism of our sensors based on mesoporous WO₃ can be explained by a surface-depletion model.^[54]

As illustrated Figure. 7a, when WO₃-based sensors are exposed to air, oxygen molecules can be chemically adsorbed on the surface of WO₃ to capture electrons from the conduction band and form adsorbed oxygen species (O₂⁻, O⁻ and O²⁻). At the same time, a thick space-charge layer is formed on the surface of WO₃, increasing the potential barriers (marked in green) with a higher resistance (Figure. 7a). In contrast, when the WO₃ sensors are exposed to 3-hydroxy-2-butanone, the target molecules can react with the adsorbed oxygen and release free electrons, which leads to the decrease of the thickness of the potential barriers (marked in green) and the electrical resistance (Figure. 7a). As shown in Figure. 7a, it can be clearly seen that large porosity and a high specific surface area of the well-crystalline ordered mesoporous WO₃-PEO₁₁₇-b-PS₁₈₆ materials can provide numerous active sites for gas adsorption, increasing the adsorbed oxygen amount. Meanwhile, the continuous crystalline framework ensures a fast transport of charge carriers from surface into bulk, leading to a high sensitivity. Since the average pore size of the synthesized mesoporous WO₃-PEO₁₁₇-b-PS₁₈₆ is around 10.6 nm, the gas molecules spread across the sensing layer can be dominated by surface diffusion,^[55, 56] resulting in the high sensitivities and selectivity.

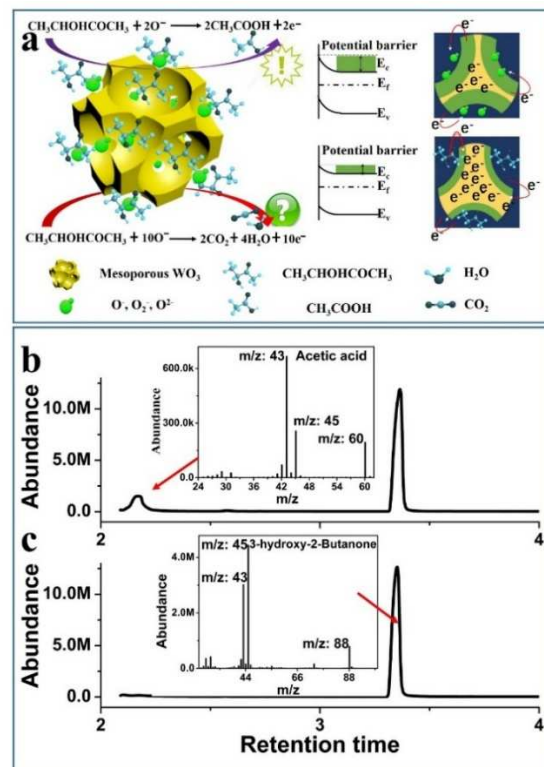
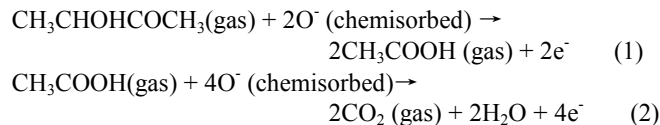


Figure 7. (a) The schematic illustration of the 3-hydroxy-2-butanone sensing mechanism of the sensors d based on mesoporous WO₃-PEO₁₁₇-b-PS₁₈₆ exposure at air and target gas-air mixture. (E_v , valence band edge; E_c , conduction band edge; E_f , Fermi energy). Gas Chromatograph-Mass Spectrometry (GC-MS) characterization of the gaseous products generated from the sensing reaction. (b) With mesoporous WO₃ inside the furnace at 290 °C, and (c) without mesoporous WO₃ inside the furnace at 290 °C.

To better understand the chemical mechanism of the WO₃ sensor for detecting the target gas, we conducted a simulated experiment to identify the products generated during sensing process. A gaseous mixture of air and 3-hydroxy-2-butanone gas was prepared and reserved in a stainless-steel cylinder (1000 ppm by volume ratio) to be allowed to pass through a tubular furnace with pre-placed WO₃ in a ceramics boat at 290 °C, and the real sensing circumstance is thus imitated. A gas-washing bottle containing ethanol as the solvent was used to collect the reaction products. The products were analyzed by GC-MS. The results show a product peak assigned to acetic acid (Figure. S10a) only when the sample mesoporous WO₃ was exposed to 3-hydroxy-2-butanone and air at 290 °C. While without the presence of WO₃ in the furnace, only 3-hydroxy-2-butanone was detected by GC even at 290 °C. The results clearly revealed that 3-hydroxy-2-butanone can be oxidized to acetic acid over WO₃ (Figure. 7b, c). The GC-MS spectra of the products generated by WO₃ materials upon exposure to 1000 ppm 3-hydroxy-2-butanone for 0.5, 1.0, 1.5, 2.0 h were also obtained (Figure. S10b). The results show a continuous accumulation of acetic acid produced by 3-hydroxy-2-butanone as the reaction proceeds. Based on the above results, it can be concluded that acetic acid is one important oxidation product of 3-hydroxy-2-butanone during sensing measurement, which is different from the conventional sensing mechanism where carbon dioxide and water are be-

1 believed to be the only two products of ketone such as acetone or
 2 n-butanol over WO₃.^[57, 58] Herein we attempted to use an elec-
 3 tron-liberate theory to explain this interesting phenomenon
 4 combining with our results. When the sensor is exposed to the
 5 reducing gases 3-hydroxy-2-butanone at a high temperature
 6 (290 °C), the species O⁻ is more important than the other oxy-
 7 gen adsorbates (O₂⁻, O²⁻),^[59, 60] and they can be readily con-
 8 sumed, releasing additional electrons, which in turn decreased
 9 the baseline resistivity by following the reactions displayed
 10 below:



11 From the above typical reactive formulas, for target gases of
 12 the same concentration, the surface reaction of acetic acid gas
 13 can release more electrons than 3-hydroxy-2-butanone, and
 14 thus the sensitivity of the sensor S_d to acetic acid should be
 15 higher than the sensor S_d to 3-hydroxy-2-butanone; however,
 16 our results (Figure. S11) indicate that the response of the S_d to
 17 3-hydroxy-2-butanone at 50 ppm (sensitivity: R_{air} / R_{gas} =
 18 498.3) is much higher than that for acetic acid at 50 ppm
 19 (sensitivity: R_{air} / R_{gas} = 14.5). Therefore, it can be concluded
 20 that, under the sensing conditions, 3-hydroxy-2-butanone
 21 predominantly follows reactions (1), and acetic acid is the
 22 oxidation product instead of carbon dioxide and water.

23 CONCLUSIONS

24 In summary, well-crystalline ordered mesoporous WO₃ with
 25 adjustable pore size of 10.6 -15.3 nm have been synthesized
 26 via a solvent evaporation induced co-assembly approach by
 27 using tailor-made PEO-*b*-PS diblock copolymers with differ-
 28 ent PS chain lengths as a template, and tungsten chloride as a
 29 precursor in the presence of chelating agent acetylacetonate.
 30 The obtained mesoporous tungsten oxides have high surface
 31 areas (76 - 136 m²/g) and adjustable pore volumes of 0.13 -
 32 0.17 cm³/g. Because of the well-connected mesoporous struc-
 33 ture with high surface areas and crystalline framework, the
 34 mesoporous WO₃-based sensors exhibit a rapid response, su-
 35 perior sensitivity and highly selective detection against 3-
 36 hydroxy-2-butanone, the biomarker for *Listeria monocyto-*
 37 *genes*, at a low concentration of sub-ppm level. The simulated
 38 on-line gas sensing analysis by GC and GC-MS indicated that
 39 the sensing performance is attributed to an unexpected new
 40 sensing mechanism of the mesoporous WO₃ chemiresistive
 41 sensor. Acetic acid is the product of 3-hydroxy-2-butanone
 42 over WO₃. A rapid, sensitive and selective sensing detection of
 43 *Listeria monocytogenes* has been achieved by using the meso-
 44 porous WO₃-based gas sensor. This new sensing concept and
 45 method hold a great promise for the development of a novel,
 46 simple, noninvasive and low-cost VOC portable sensor device
 47 for the detection of alive and active foodborne bacteria in clin-
 48 ical and food samples.

49 ASSOCIATED CONTENT

50 Supporting Information.

51 The structure of the sensor and working principle of the gas
 52 sensing measurement system. ¹H NMR spectra of PEO-Br and
 53 the synthesized diblock copolymer PEO-*b*-PS. The gel perme-
 54 ation chromatograph (GPC) trace of diblock copolymer PEO-
 55 *b*-PS. Window-size distribution curves of WO₃-PEO_x-*b*-PS_y
 56 samples obtained after carbonization in N₂ at 350 °C and cal-
 57 cination at 500 °C in air (1) WO₃-PEO₁₁₇-*b*-PS₂₉₇, (2) WO₃-
 58 PEO₁₁₇-*b*-PS₂₃₂, (3) WO₃-PEO₁₁₇-*b*-PS₁₈₆. XRD patterns of (a)
 59 commercial WO₃ particles, and WO₃-PEO_x-*b*-PS_y samples
 60 obtained after carbonization in N₂ at 350 °C and calcination at
 500 °C in air, (b) WO₃-PEO₁₁₇-*b*-PS₂₉₇, (c) WO₃-PEO₁₁₇-*b*-
 PS₂₃₂, (d) WO₃-PEO₁₁₇-*b*-PS₁₈₆. The high-resolution X-ray
 photoelectron spectroscopy (XPS) of WO₃-PEO₁₁₇-*b*-PS₁₈₆
 samples obtained after carbonization in N₂ at 350 °C and fur-
 ther calcination at 500 °C in air. (a) W 4f for WO₃-PEO₁₁₇-*b*-
 PS₁₈₆, (b) O 1s for WO₃-PEO₁₁₇-*b*-PS₁₈₆. Raman spectra of (a)
 commercial WO₃ particles, and WO₃-PEO_x-*b*-PS_y samples
 obtained after carbonization in N₂ at 350 °C and calcination at
 500 °C in air, (b) WO₃-PEO₁₁₇-*b*-PS₂₉₇, (c) WO₃-PEO₁₁₇-*b*-
 PS₂₃₂, (d) WO₃-PEO₁₁₇-*b*-PS₁₈₆. The long-term stability of the
 sensors base on different samples (S_a, S_b, S_c, and S_d based on
 commercial WO₃ particles, WO₃-PEO₁₁₇-*b*-PS₂₉₇, WO₃-
 PEO₁₁₇-*b*-PS₂₃₂, and WO₃-PEO₁₁₇-*b*-PS₁₈₆, respectively). The
 growth kinetics of *Listeria monocytogenes* at different initial
 concentration of (a) 10¹, (b) 10², (c) 10³ CFU mL⁻¹ using plate
 count enumeration. Three trials with three replicates per trial
 were done for each temperature. The sensing response of S_d
 based on WO₃-PEO₁₁₇-*b*-PS₁₈₆ upon exposure to 10⁶ CFU
 mL⁻¹ *Vibrio parahaemolyticus*, 10⁶ CFU mL⁻¹ *Escherichia*
coli and 10³ CFU mL⁻¹ *Listeria Monocytogenes*. A series of
 experiments results indicate that only the sample exposed to 3-
 hydroxy-2-butanone and air at 290 °C. (b) Gas Chromato-
 graph-Mass Spectrometry (GC-MS) characterization of the
 gaseous products generated from the sensing reaction at dif-
 ferent time. Responses of sensor S_d based on WO₃-PEO₁₁₇-*b*-
 PS₁₈₆ to 3-hydroxy-2-butanone and acetic acid gases at 50 ppm,
 respectively.
 This material is available free of charge via the Internet at
<http://pubs.acs.org>.

51
52
53
54
55
56
57
58
59
60

AUTHOR INFORMATION

Corresponding Author

* yhdeng@fudan.edu.cn

Author Contributions

[†]ZYH and ZY contribute equally to this study. The manuscript
 was written by contributions of all authors.

Notes

The authors declare no competing financial interest.

ACKNOWLEDGMENT

This work was supported the NSF of China (51372041,
 51422202, 51402049 and 51432004), the “Shu Guang” Project
 (13SG02) supported by Shanghai Municipal Education Com-
 mission and Shanghai Education Development Foundation,
 Shanghai Sci. & Tech. Committee (14JC1400700), Youth
 Top-notch Talent Support Program of China, China Post-
 doctoral Science Foundation (KLH1615138), Shanghai Nature
 Science Foundation of China (14ZR1416600) and the state
 key laboratory of Transducer Technology of China (Grant No.
 SKT1503). The authors extend their appreciation to the Inter-
 national Scientific Partnership Program ISPP at King Saud

University for funding this research work through ISPP# 0094. The authors thank Prof. Guangrong Zhou for assistance in TEM characterization.

REFERENCES

- (1) Elaine, S.; Robert, M. H.; Frederick, J. A.; Robert, V. T.; Marc, A. W. *Emerg Infect Dis*, **2011**, 17, 7 - 15.
- (2) Hamon, M.; Bierne, H.; Cossart, P. **2006**, 4, 423-434.
- (3) Paolo, A.; Gionvanni, C. F.; Daniela, C.; Gionvanna M.; Oreste N.; Leonello L.; Stefania S. *New Engl J Med*, **2000**, 341, 1236 - 1241.
- (4) Welch, M. D.; Rosenblatt, J.; Skoble, J.; Portnoy, D. A.; Mitchison, T. J. *Science*, **1998**, 281, 105 - 108.
- (5) Olivier L.; Javier D. C.; Xavier M. *Biosens. Bioelectron.*, **2007**, 22, 1205 - 1217.
- (6) Vijayalakshmi, V.; Khalil, A.; Olga, K.; Kamila, O.; Catherine A. *Biotechnol Adv*, **2010**, 28, 232 - 254.
- (7) Li, Y.G.; Cu, R. T.; Luo, D. *Nat. Biotechnol*, **2005**, 23, 885 - 889.
- (8) Wang, R.H.; Ruan, C. M.; Kanayeva, D.; Lassiter, K.; Li, Y. B. *Nano Lett.*, **2008**, 8, pp 2625 - 2631.
- (9) Wang Y.; Li Y. X.; Yang, J. L.; Ruan, J.; Sun, C. J. *Trends in Anal.Chem*, **2016**, 78, 1 - 16.
- (10) Kim, S. J.; Choi, S. J.; Jang, J. S.; Kim, N. H.; Hakim, M.I.; Tuller, H. L.; Kim, I. D. *ACS Nano*, **2016**, 10, 5891 - 5899.
- (11) Yang, W.; Wan, P.; Jia, M.; Hu, J.; Guan, Y.; Feng, L. *Biosens. Bioelectron.*, **2015**, 64, 547 - 553.
- (12) Turner, A. P.; Magan, N. *Nat. Rev. Microbiol.*, **2004**, 2, 161 - 166.
- (13) Shin, J.; Choi, S. J.; Lee, I.; Youn, D. Y.; Park, C. O.; Lee, J. H.; Tuller, H. L.; Kim, I. D. *Adv. Funct. Mater.*, **2013**, 23, 2357 - 2367.
- (14) Gobbi, E.; Falasconi, M.; Zambotti, G.; Sberveglieri, V.; Pulvirenti, A.; Sberveglieri, G. *Sens. Actuators B*, **2015**, 207, 1104 - 1113.
- (15) Lippolis, V.; Ferrara, M.; Cervellieri, S.; Damascelli, A.; Epifani, F.; Pascale, M.; Perrone, G. *Int. J. Food Microbiol.*, **2016**, 218, 71 - 77.
- (16) Carmona, E. N.; Sberveglieri, V.; Ponzoni, A.; Galstyan, V.; Zappa, D.; Pulvirenti, A.; Comini, *Sens. Actuators B*, **2017**, 238, 1224 - 1230.
- (17) Korpi, A.; Jarnberg, J.; Pasanen, A. *Crit. Rev. Toxicol.*, **2009**, 39, 139 - 193.
- (18) Deshmukh, S.; Bandyopadhyay, R.; Bhattacharyya, N.; Pandey, R. A.; Jana, A. *Talanta*, **2015**, 144, 329 - 340.
- (19) Broza, Y. Y.; Haick, H. *Nanomedicine*, **2013**, 8, 785 - 806.
- (20) Xu, C.; Tamaki, J.; Miura, N.; Yamazoe, N. *Sens. Actuators B*, **1991**, 3, 147-155
- (21) Li, Y. H.; Luo, W.; Qin, N.; Dong, J. P.; Wei, J.; Li, W.; Feng, S. S.; Chen, J. C.; Xu, J. Q.; Elzatahry, A. A.; Es-Saheb, M. H.; Deng, Y. H.; and Zhao, D. Y. *Angew. Chem. Int. Ed.*, **2014**, 53, 9035 - 9040.
- (22) Wang, Z. R.; Zhu, Y. H.; Luo, W.; Ren, Y.; Cheng, X. W.; Xu, P. C.; Li, X. X.; Deng, Y. H.; Zhao, D. Y. *Chem. Mater.*, **2016**, 28, 7773 - 7780.
- (23) Ren, Y.; Zhou, X. R.; Luo, W.; Xu, P. C.; Zhu, Y. H.; Li, X. X.; Cheng, X. W.; Deng, Y. H.; Zhao, D. Y. *Chem. Mater.*, **2016**, 28, 7997 - 8005.
- (24) Zhou, X. R.; Zhu, Y. H.; Luo, W.; Ren, Y.; Xu, P. C.; Elzatahry, A. A.; Cheng, X. W.; Abdulaziz, A.; Deng, Y. H.; Zhao, D. Y. *J. Mater. Chem. A*, **2016**, 4, 15064 - 15071.
- (25) Yang, P. D.; Zhao, D. Y.; Margolese, D. I.; Chmelka, B. F.; and Stucky, G. D. *Nature*, **1998**, 396, 152 - 155.
- (26) Li, L.; Krissanasaerane, M.; Pattinson, S. W.; Stefik, M.; Wiesner, U.; Steiner, U.; Eder, D. *Chem. Commun.*, **2010**, 46, 7620 - 7622.
- (27) Lokupitiya, H. N.; Jones, A.; Reid, B.; Guldin, S.; Stefik, M. *Chem. Mater.* **2016**, 28, 1653 - 1667.
- (28) Jo, C.; Hwang, J.; Song, H.; Dao, A. H.; Kim, Y.; Lee, S. H.; Hong, S. E.; Yoon, S.; Lee, J. *Adv. Funct. Mater.* **2013**, 23, 3747 - 3754.
- (29) Tiemann, M. *Chem. Eur. J.*, **2007**, 13, 8376 - 8388.
- (30) Koo, W. T.; Choi, S. J.; Kim, S. J.; Jang, J. S.; Tuller, H. L. and Kim, I. D. *J. Am. Chem. Soc.*, **2016**, 138, 13431 - 13437.
- (31) Wang, Z.; Tian, Z.; Han, D.; Gu, F. *ACS Appl. Mater. Interfaces*, **2016**, 8, 5466 - 5474.
- (32) Sakai, G.; Matsunaga, N.; Shimanoe, K.; Yamazoe, N. *Sens. Actuators B*, **2001**, 80, 125 - 131.
- (33) Pinna, N.; Neri, G.; Antonietti, M.; Niederberger, M. *Angew. Chem. Int. Ed.*, **2004**, 43, 4345 - 4349.
- (34) Cabota, A.; Arbiola, J.; Morantea, J. R.; Weimarb, U.; Bàrsanb, N.; Göpel, W. *Sens. Actuators B*, **2000**, 70, 87 - 100.
- (35) Korotcenkov, G.; Blinov, I.; Ivanov, M.; Stetter, J. R. *Sens. Actuators B*, **2007**, 120, 679 - 686.
- (36) Liu, Y.; Koep, E. and Liu, M. A. *Chem. Mater.*, 2005, 17, 3997 - 4000.
- (37) Deng, Y. H.; Yu, T.; Wan, Y.; Shi, Y.; Meng, Y.; Gu, D.; Zhang, L.; Huang, Y.; Liu, C.; Wu, X.; Zhao, D. Y. *J. Am. Chem. Soc.*, **2007**, 129, 1690 - 1697.
- (38) Fan, J.; Yu, C. Z.; Gao, F.; Lei, J.; Tian, B. Z.; Wang, L. M.; Luo, Q.; Tu, B.; Zhou, W. Z.; Zhao, D. Y. *Angew. Chem. Int. Ed.*, **2003**, 42, 3146 - 3150.
- (39) Jiang, B.; Li, C.; Tang, J.; Takei, T.; Kim, J. H.; Ide, Y.; Henzie, J.; Tominaka, S.; Yamauchi, Y. *Angew. Chem. Int. Ed.*, **2016**, 55, 10037 - 10041.
- (40) Bastakoti, B. P.; Ishihara, S.; Leo, S. Y.; Ariga, K.; Wu, K. C.; Yamauchi, Y. *Langmuir*, **2014**, 30, 651 - 659.
- (41) Tang, J.; Liu, J.; Li, C.; Li, Y.; Tade, M. O.; Dai, S.; Yamauchi, Y. *Angew. Chem. Int. Ed.*, **2015**, 54, 588 - 593.
- (42) Luo, W.; Zhao, T.; Li, Y. H.; Wei, J.; Xu, P. C.; Li, X. X.; Wang, Y. W.; Zhang, W. Q.; Elzatahry, A. A.; Alghamdi, A.; Deng, Y. H.; Wang, L. J.; Jiang, W.; Liu, Y.; Kong, B. and Zhao, D. Y. *J. Am. Chem. Soc.*, **2016**, 138, 12586 - 12595.
- (43) Wei, J.; Deng, Y. H.; Zhang, J. Y.; Sun, Z. K.; Tu, B.; Zhao, D. Y. *Solid State Sci*, **2011**, 13, 784 - 792.
- (44) Santato C.; Odziemkowski, M.; Ulmann, M.; Augustynski, J. *J. Am. Chem. Soc.*, **2001**, 123, 10639 - 10649.
- (45) Choi, S. J.; Choi, C.; Kim, S.-J.; Cho, H.-J.; Hakim, M.; Jeon, S.; Kim, I. D. *Sci. Rep.*, **2015**, 5, 8067 - 8091.
- (46) Aono, H.; Traversa, E.; Sakamoto, M.; Sadaoka, Y. *Sens. Actuators B*, **2003**, 94, 132 - 139.
- (47) Wang, L.; Teleki, A.; Pratsinis, S. E. and Gouma, P. I. *Chem. Mater.*, **2008**, 20, 4794 - 4796.
- (48) Wang, L. C.; Wang, Y.; Cheng, Y.; Liu, Z. F.; Guo, Q. S.; Hac, M. N. and Zhao, Z. *J. Mater. Chem. A*, **2016**, 4, 5314 - 5322.
- (49) Wagner, T.; Haffer, S.; Weinberger, C.; Klaus, D.; Tiemann, M. *Chem. Soc. Rev.*, **2013**, 42, 4036 - 4053.
- (50) Kukkola, J.; Mäklin, J.; Halonen, N.; Kyllönen, T.; Tóth, G.; Szabó, M.; Shchukarev, A.; Mikkola, J. P.; Jantunen, H.; Kordás, K. *Sens. Actuators B*, **2011**, 153, 293 - 300.
- (51) Yu, Y. X.; Sun, X. H.; Liu, Y.; Pan, Y. J. and Zhao, Y. *J. Microbiol.*, **2015**, 61, 367 - 372.
- (52) Adami, A.; Lorenzelli, L.; Guarnieri, V.; Francioso, L. A.; Forleo, G.; Agnusdei, A. M.; Taurino, M.; Zen, P.; Siciliano, A. *Sens. Actuators B*, **2006**, 117, 115 - 122.
- (53) Jing, Z.; Zhan, J. *Adv. Mater.*, **2008**, 20, 4547 - 4551.
- (54) Sakai, G.; Matsunaga, N.; Shimanoe, K.; Yamazoe, N. *Sens. Actuators B*, **2001**, 8, 125 - 131.
- (55) Ogawa, H.; Nishikawa, M. and Abe, A. *J. Appl. Phys.*, **1982**, 53, 4448 - 4455.
- (56) Labidi, A.; Lambert-Mauriat, C.; Jacolin, C.; Bendahan, M.; Maaref, M.; Aguir, K. *Sens. Actuators B*, **2006**, 119, 374 - 379.
- (57) Malik, R.; Tomer, V. K.; Chaudhary, V.; Dahiya, M. S.; Nehra, S. P.; Rana, P. S.; Duhan, S. *Sens. Actuators B*, **2017**, 239, 364 - 373.
- (58) Liu, Z.; Liu, B.; Xie, W.; Li, H.; Zhou, R.; Li, Q. H.; Wang, T.

H. *Sens. Actuators B*, **2016**, 235, 614 - 621.

- (59) Franke, M. E.; Koplín, T. J.; Simon, U. *Small*, **2006**, 2, 36 - 50.
(60) Yamazoe N.; Sakai G.; Shimanoé, K. *Catal Surv Asia*, **2003**, 7,
63 - 75.

1
2
3
4
5
6
7
8
9
10
11
12
13
14
15
16
17
18
19
20
21
22
23
24
25
26
27
28
29
30
31
32
33
34
35
36
37
38
39
40
41
42
43
44
45
46
47
48
49
50
51
52
53
54
55
56
57
58
59
60

TOC graphic

